Current-voltage characteristic in narrow channels and low-voltage breakdown of the quantum Hall effect

O. G. Balev
Institute of Physics of Semiconductors, Academy of Sciences, 45 Prospekt Nauky, Kiev 252650, Ukraine

P. Vasilopoulos
Department of Physics, Concordia University, 1455 de Maisonneuve Boulevard O, Montréal, Québec, Canada, H3G 1M8

E. V. Mozdor
Institute of Physics of Semiconductors, Academy of Sciences, 45 Prospekt Nauky, Kiev 252650, Ukraine
(Received 23 March 1994)

Low-voltage breakdown of the quantum Hall effect is considered in narrow quasi-two-dimensional channels subjected to a strong perpendicular magnetic field. The interaction of electrons with acoustical (deformation or piezoelectric) phonons leads to a substantial dissipation at the edges of the channel, due to electron transitions between the edges states. It is the main dissipation if the channel width W is not too large. Nonheating negative differential conduction, $dj_x/dE_x < 0$, when an electric field E_x is applied along the channel, is possible for drift velocities v_D smaller ($v_D < s$) or much smaller ($v_D << s$) than the speed of sound s as well for $v_D > s$. The current-voltage characteristic (CVC) $j_x = j_x(E_x)$, evaluated numerically for a number of qualitatively different cases, is substantially nonlinear if v_D is not too small. The results are in good agreement with the experimental results by von Klitzing *et al.* for low breakdown velocities ($v_D \sim s/20$) in metal-oxide-semiconductor (MOS) structures. An increase by orders of magnitude in the dissipation, before breakdown, as observed, e.g., by Komiyama *et al.* is explained as well. The anisotropy of the electron-phonon interaction in MOS structures and its substantial influence on the CVC and breakdown velocities is also considered. The dissipation depends very strongly on the frequency Ω of the confining potential if v_D is not too large. In contrast with Martin and Feng [Phys. Rev. Lett. **64**, 1971 (1990)], for sufficiently small Ω, an exponential suppression of the dissipation occurs due to intralevel-intraedge acoustic-phonon-assisted transitions.

I. INTRODUCTION

The understanding of the breakdown the quantum Hall effect (QHE) still evolves as more experimental and theoretical results are obtained. A comprehensive review of the literature on this breakdown is given in Ref. 3 and earlier reviews are given in Refs. 4 and 5. The breakdown is usually associated with electron-phonon interaction.[4–6] Reference 6 proposed another theory of the breakdown of the QHE in wide channels. It is associated with a nonheating negative differential conductivity under electron-phonon interaction, if the drift velocity $v_D = E_y/B$ is larger or equal to the speed of sound s that leads to an instability of the almost dissipationless regime. Here B is the magnetic field, and $E_y = E_H$ the Hall field.

For narrow channels, when the main dissipation is due to the electron-phonon interaction related with electron transitions at the edges of the channel, it has been shown[7] that low-voltage breakdown, due to negative differential conduction (NDC), is possible for $v_D < s$ and in particular $v_D \ll s$. In Ref. 7 the current-voltage characteristic (CVC) with NDC in analytic form was obtained only for $v_D \gtrsim s/4$, if fluctuations in the confining potential are neglected. This agrees well with the maximum values of a threshold drift velocity v_D in many experiments on GaAs/(AlGa)As heterostructures.[2–5,8] In addition, some essential features of an experiment[8] were explained. However, in some interesting cases the behavior of the CVC could be estimated only very approximately, e.g., the possibility of breakdown related with NDC in some ranges of v_D. This treatment cannot be applied directly to the experimental conditions of Refs. 1 and 9 where in a Si(100) metal-oxide-semiconductor (MOS) structure with channel width 80 μm (Ref. 1) and 10 μm (Ref. 9) the maximum v_D for breakdown was about $s/20$ (see also Ref. 5), i.e., much lower than the speed of sound $s = 8.4 \times 10^5$ cm/sec in silicon.[9,10] This drawback of the analytical treatment is related with the absence of a small parameter $\Delta E/\bar{E} \ll 1$, where $\Delta E = \Delta E_H$ gives an estimate of the possible NDC region and $\bar{E} = \bar{E}_H$ is the typical value of E_H in that region,[7] see also below. Here, apart from a numerical treatment of CVC's in qualitatively interesting cases, which cannot be studied analytically, we also take into account the anisotropy of the electron-phonon interaction in Si(100) MOS structures.[11] Due to this anisotropy, in some cases the interaction with TA phonons is more important than that with LA phonons in determining the CVC. Moreover, the anisotropy can enlarge the region of NDC or promote its appearence in new regions in comparison

with the case where this interaction is isotropic.

The possibility of low-voltage breakdown due to electron-phonon interaction at the edges of the channel is related with finite but not too high temperatures.[7] Physically, in a narrow channel electron states (and transitions between them) are more pertinent at the edges of the channel than at its interior. Indeed, at the edges of the channel the Landau levels are tilted upwards by the confining potential and the Fermi level crosses them. So the states in the vicinity of the edges are close to the Fermi level and at low temperatures they contribute to dissipation, via the electron-phonon interaction, much more than the "bulk" states (at the interior of the sample) since they lie far below the Fermi level. In fact, it has been observed[6] that the contribution of these inner states, lying $\Delta_{\rm in}$ below the Fermi level, decreases exponentially with temperature if the condition $\exp(-\Delta_{\rm in}/k_BT) \ll 1$ is satisfied.

Following Ref. 7 we will study the breakdown of the QHE in a narrow channel, of finite thickness and of infinite length, in the presence of a strong perpendicular magnetic field B such that $\hbar\omega_c \gg k_BT$, where $\omega_c = |e|B/m^*$ is the cyclotron frequency, m^* the effective mass, and $e(<0)$ the electron charge. We neglect a random static potential as well as the interaction between electrons. The only scattering we consider is electron-phonon interaction in relatively weak applied electric fields (along the channel) when the condition $|E_x/E_H| \ll 1$ is satisfied due to the strong magnetic field. The heating of the two-dimensional electron gas (2DEG) is neglected. We assume that E_H is not large enough to cause interlevel transitions. In the case of Si MOS structures we take the z axis along the $\langle 100\rangle$ direction.

The paper is organized as follows. In Sec. II we present some basic relations from Ref. 7, for the convenience of the reader, and additional formalism related with the anisotropy of the electron-phonon interaction in Si(100) MOS structures. In Sec. III we calculate the CVC for the isotropic electron-phonon interaction. In Sec. IV we treat the influence of the anisotropy of this interaction on the CVC for Si(100) MOS structures. Finally, in Sec. V we present a discussion and the concluding remarks.

II. BASIC RELATIONS

A. Channel characteristics

We consider a 2DEG confined in a narrow channel, in the (x,y) plane, of width W, of length L, and of finite thickness d. For $W \lesssim 0.1$ μm we can take the confining potential along y as parabolic: $V_y = m^*\Omega^2 y^2/2$, where Ω is the confining frequency. However, as explained in Ref. 7, all the results can be directly extended to the more realistic potential ($W \gtrsim 1$ μm) $V'_y = 0$ for $y_l < y < y_r$, $V_y' = m^*\Omega^2(y-y_r)^2/2$ for $y > y_r > 0$, and $V'_y = m^*\Omega^2(y-y_l)^2/2$ for $y < y_l < 0$. We point out that y_l and y_r are not exactly the left and right edges of the channel. However, for $W > 1$ μm, we have $W \approx y_r - y_l$, see also Ref. 12. Below, we will consider mostly this case; the results can be easily extended to the case of V_y. For the confinement in the z direction we consider a parabolic well of frequency ω_z or the standard triangular well. As explained in Ref. 7, when an electric field E_x is applied along the channel and a strong magnetic field B along the z axis we should include the Hall field E_H in the one-electron Hamiltonian. The components of the current density averaged over a statistical ensemble and the dimensions of the channel are given by[7]

$$j_y = \sigma_{yy}(E_H)E_H + \sigma^0_{yx}E_x = 0, \tag{1}$$

$$j_x \approx \sigma^0_{xy}E_H. \tag{2}$$

Here, the superscript 0 in $\sigma^0_{yx} = -\sigma^0_{xy} \propto e^2/2\pi\hbar$ denotes the absence of electron-phonon interaction. The term $\sigma_{yy}(E_H)E_H$ in Eq. (1), labeled j_d to remind that it expresses the dissipation, is given, when only the lowest Landau Level ($N=0$) is occupied, for isotropic electron-phonon interaction by

$$j_d = \sigma_{yy}(E_H)E_H = \frac{|e|\omega_c c'}{4\pi^2\hbar s m^*\tilde\omega^2 W}\int_{-\infty}^{\infty}\int_{-\infty}^{\infty} dq_x dk_x q_x [q_x\tilde v]^{m+1}[f(E_0(k_x)) - f(E_0(k_x-q_x))]$$
$$\times\left\{\frac{1}{1-e^{[E_0(k_x)-E_0(k_x-q_x)]/k_BT}} - \frac{1}{1-e^{\hbar s q_x\tilde v/k_BT}}\right\}$$
$$\times I_0(q_x^2\tilde\ell^2\lambda_-(\tilde v^2-1)/4)e^{-q_x^2\tilde\ell^2[1+\lambda_+(\tilde v^2-1)/2]/2}, \tag{3}$$

where $E_0(k_x) = \hbar\tilde\omega/2 + \hbar^2k_x^2/2\tilde m + E_{z0}$ and

$$q_x\tilde v > 0, \quad \tilde v^2 > 1\,. \tag{4}$$

Here c' is a constant related with the strength of electron-phonon interaction $C_{\vec q}$, $\tilde\omega = (\omega_c^2+\Omega^2)^{1/2}$, $\tilde m = m^*\tilde\omega^2/\Omega^2$, and E_{z0} is the eigenvalue of the lowest subband related with quantization of motion in the z direction. In line with most experimental situations we assume that the 2DEG occupies only this level. Further, $m = 1$ or -1 for standard acoustical (DA) or piezoelectrical (PA) phonons, $C_{\vec q}^2 = (c'/L_xL_yL_z)q^{\pm1}$, and $\omega_q = sq$ is the phonon frequency, $q = (q_x^2+q_y^2+q_z^2)^{1/2}$. Moreover, $f(E_0(k_x)) = 1/(1+\exp\{[E_0(k_x)-E_F]/k_BT\})$ is the Fermi-Dirac function, E_F is the Fermi level, $I_0(x)$ is the modified Bessel function, $\tilde v = v - (\hbar q_x/2m^*s)(\Omega/\tilde\omega)^2$, $\tilde\ell = (\hbar/m^*\tilde\omega)^{1/2}$ is the renormalized magnetic length, and $\lambda_\pm = 1 \pm \ell_z^2/\tilde\ell^2$. The factor $v \equiv v(k_x,k_E) = \hbar(k_x + k_E)/\tilde m s$ is a dimensionless number which, for $\Omega \to 0$, reduces to the ratio of the drift velocity to that of sound, $v \to E_H/sB$, and $k_E = |e|\omega_cE_H/\hbar\Omega^2$. For d finite and

$V_z = m^*\omega_z^2 z^2/2$ we have $\ell_z^2 = \hbar/m^*\omega_z \ll \tilde{\ell}^2$ if $\omega_z \gg \tilde{\omega}$. For typical values $\bar{q}_z^2 \ll \ell_z^{-2}$ the result for matrix element[7] $F(q_z)$ is almost equal to that obtained from the variational wave function $X_0(z) = z(b_0^3/2)^{1/2}\exp(-b_0 z/2)$ if $\ell_z^{-2} = b_0^2/6$, i.e., $F(q_z) = [1 + q_z^2/b_0^2]^{-3}$; in this case the average thickness is $3/b_0$. In the former case $F(q_z) = \exp(-q_z^2\ell_z^2/2)$.

As a rule we will calculate Eq. (3) numerically and compare the results with those of Ref. 7 or our new analytical ones. Then we will need the characteristic wave number[7] $k_e = (\tilde{\omega}/\hbar\Omega)[2m^*\Delta_F]^{1/2}$, where $\Delta_F = (E_{F0} - \hbar\tilde{\omega}/2)$ and $E_{F0} = E_F - E_{z0}$; in the case of parabolic potential V_y channel width $W = 2\hbar\omega_c k_e/m^*\tilde{\omega}^2$, i.e., it is proportional to k_e. Notice that in the latter case $f(E_0(\pm k_e)) = 1/2$; thus k_e corresponds to the intersection of the Fermi level and of the Landau level. It can be seen that k_e determines the characteristic electric field $E_e = \hbar\Omega^2 k_e/|e|\omega_c$ defining the influence of the channel boundaries (see also below) on the edge states.

From Eqs. (1) and (3) we can express E_H as function of E_x, $E_H = E_H(E_x)$. Then from Eq. (2) the CVC, $j_x = j_x(E_x)$, and the condition for NDC, $\partial j_x/\partial E_x < 0$, are written as

$$j_x = \sigma_{xy}^0 E_H(E_x), \tag{5}$$

and

$$\frac{\partial j_d}{\partial E_H}|_{E_H(E_x)} < 0, \tag{6}$$

respectively. Criterion (6), which follows from $\partial j_x/\partial E_x < 0$ and Eqs. (1)–(3), is a condition for the breakdown of the QHE. The more general condition $j_d \neq 0$, which leads to a weakly dissipative regime and is necessary for breakdown as well, is treated numerically. We will assume $\Omega \ll |\omega_c|$, i.e., that the confining potential affects the eigenfunctions very little but it substantially changes the eigenvalues. This condition is usually fulfilled if the magnetic field is not too weak,[7,13] for more details see Sec. V. We also assume that E_H is not strong enough to cause interlevel transitions.

From Eqs. (1) and (2) it follows $j_d E_H = j_x E_x$, i.e., after determining j_d it is not difficult to obtain dissipation in the channel. Because of the relationship $E_x = j_d(E_H)/\sigma_{xy}^0 = \sigma_{yy}(E_H)E_H/\sigma_{xy}^0$, the construction of the CVC $E_x = E_x(j_x)$ is equivalent, in relative units, to that of the dependence $j_d = j_d(E_H)$. We have the resistivity $\rho_{xx} = E_x/j_x \approx j_d/E_H(\sigma_{yx}^0)^2$. For definiteness, we will suppose $E_H > 0, B > 0$. In Eqs. (1) and (2) we have $\sigma_{yx}^0 = e^2/2\pi\hbar$. For simplicity we neglect the spin and valley dependence of the filling factor[1] ν unless stated otherwise.

B. Anisotropic electron-phonon interaction

In Si(100) MOS structures we have, for LA and TA phonons, respectively, $|C_{\vec{q}}|^2$ in the form[11,14] $B_{0L}\, q(-a_L + q_z^2/q^2)^2/V$ and $B_{0T}\, q(q_z^2/q^2)(1 - q_z^2/q^2)/V$, where $V = L_x L_y L_z$, $a_L = -\Xi_d/\Xi_u = 2/3$, $\Xi_d = -6$ eV, $\Xi_u = 9$ eV, $B_{0L,T} = \hbar\Xi_u^2/2\rho s_{L,T}$, and ρ is the density of crystal. For interaction with LA (TA) phonons s_L (s_T) is the corresponding sound veloscity. Then for LA and TA phonons, when only the lowest Landau level $N = 0$ is filled, we obtain

$$j_d^{L,T} = \frac{|e|\omega_c B_{0L,T}}{4\pi^2\hbar s_{L,T} m^*\tilde{\omega}^2 W}\int_{-\infty}^{\infty}\int_{-\infty}^{\infty} dq_x dk_x q_x^3 [f(E_0(k_x)) - f(E_0(k_x - q_x))]$$

$$\times\left\{\frac{1}{1 - e^{[E_0(k_x) - E_0(k_x - q_x)]/k_B T}} - \frac{1}{1 - e^{\hbar s q_x \tilde{v}/k_B T}}\right\} e^{-q_x^2\tilde{\ell}^2[1 + (\lambda_+ - 1)(\tilde{v}^2 - 1)]/2}$$

$$\times\{A_1^{L,T}\tilde{v}^2 I_0(q_x^2\tilde{\ell}^2\lambda_-(\tilde{v}^2 - 1)/4)e^{-q_x^2\tilde{\ell}^2\lambda_-(\tilde{v}^2-1)/4}$$

$$+A_2^{L,T}(\tilde{v}^2 - 1)\Phi(\tfrac{1}{2}, 2; -q_x^2\tilde{\ell}^2\lambda_-(\tilde{v}^2 - 1)/2) + A_3^{L,T}(\tilde{v}^2 - 1)^2\tilde{v}^{-2}\Phi(\tfrac{1}{2}, 3; -q_x^2\tilde{\ell}^2\lambda_-(\tilde{v}^2 - 1)/2)\}, \tag{7}$$

where $\Phi(\alpha, \gamma; z)$ is the confluent hypergeometric function.[15] Further, $A_1^L = a_L^2$, $A_1^T = 0$, $A_2^L = -a_L$, $A_2^T = 1/2$, $A_3^L = 3/8$, $A_3^T = -3/8$, and conditions (4) are imposed. We will use the values[9,10] $s_L = 8.4 \times 10^5$ cm/sec and[11] $s_T = 5.8 \times 10^5$ cm/sec.

Notice that Eq. (7), for LA phonons, coincides with Eq. (3) if we suppose $\Xi_u \to 0$ and hence $a_L \to \infty$ and $B_{0L}a_L^2 \to c'$. An analytical treatment of Eq. (7) shows that the anisotropy of the electron-phonon interaction leads to a NDC at least for low voltages. If we take $1/\ell_z^2 = b_0^2/6$ we obtain[7] $\tilde{\ell}^2/\ell_z^2 \gtrsim 1$ in line with usual experimental conditions.

III. ISOTROPIC ELECTRON-PHONON INTERACTION

First, we will study how the suppression of the dissipation at the left edge of the channel ($y_{LE} = -\hbar\omega_c k_e/m^*\tilde{\omega}^2 < 0$, for V_y) affects the CVC with increasing E_H for $E_e > E_s$; here $E_s = \tilde{\omega}^2 sB/\omega_c^2$. As pointed out in Ref. 7, this can in principle lead to NDC in the low-voltage region. In Fig. 1 we represent the CVC for $T = 1.7$ K, $B = 10$ T, and $s = 7.1 \times 10^5$ cm/sec, $m^* = 10^{-28}$ g. Here the material parameters are intermediate between those of a Si MOS structure and

those of a $GaAs/Al_xGa_{1-x}As$ heterostructure. We do this to demonstrate the difference in the CVC between DA phonons (two dashed curves) and PA phonons (two solid curves) for similar conditions. In Fig. 1 the upper dashed (solid) curve corresponds to $t = (\lambda_+ - 1)^{-1} = 2$ and the lower dashed (solid) curve to $t = 1$. We have taken $D = \Omega^2/\tilde{\omega}^2 = 5 \times 10^{-3}$, $\tilde{\Delta} = \Delta_F/k_BT = 26$, $g = \hbar\tilde{\omega}/k_BT = 68$, and $x_T = \hbar s/\tilde{\ell}k_BT = 3.84$. We have also introduced the dimensionless electric fields $\tilde{E}_H = k_E\tilde{\ell} = E_H/(\hbar\Omega^2/|e|\omega_c\tilde{\ell})$, $\tilde{E}_s = E_s/(\hbar\Omega^2/|e|\omega_c\tilde{\ell}) = x_T/gD$. Notice that $\tilde{E}_H = \tilde{E}_s$ (as well as $E_H = E_s$) corresponds to $v_D = s$, if we neglect small corrections $\propto \Omega^2/\tilde{\omega}^2$. As pointed out in Ref. 7, for $E_e > E_s$ and

$$\frac{\bar{E}}{E_s} = \frac{E_e}{E_s} - 1 = (2\tilde{\Delta}Dg/x_T^2)^{1/2} - 1 \tag{8}$$

we can have NDC in the characteristic region $\Delta E_H \approx \Delta E$ with $\bar{E}$ lying approximately in this region. For $x_T \gg 1$ we have

$$\Delta E/E_s = \max\{\Omega^2 k_BT/m^*s^2\tilde{\omega}^2, k_BT/\hbar sk_e\}, \tag{9}$$

and for $x_T \lesssim 1$ we have

$$\Delta E/E_s = \max\{\hbar\Omega^2/m^*s\tilde{\ell}\tilde{\omega}^2, k_BT/\hbar sk_e\}. \tag{10}$$

Then for Fig. 1 we obtain from Eqs. (8) and (9) $\bar{E}/E_s = 0.095$, $\Delta E/E_s = \Delta v_D/s = 2.3 \times 10^{-2}$, and $\Delta E/\bar{E} \approx 0.24$. These estimates are in good agreement with Fig. 1. Indeed, both CVC's for interaction with PA phonons represent NDC for $0.10 \leq v_D/s \leq 0.14$, i.e., in the region of E_H that compares well with estimates obtained from Eqs. (8) and (9). As can be seen in Fig. 1, in this region both CVC's for DA phonons do not show NDC. However, their dependence $E_x = E_x(j_x)$ becomes already very sublinear or even (for $t = 1$) quasiflat. We can see from Fig. 1 that the finite thickness of the channel (i.e., smaller t) promotes the appearence of the NDC region. This is similar to the dependence of the breakdown velocity v_D on d in the cases treated in Ref. 7.

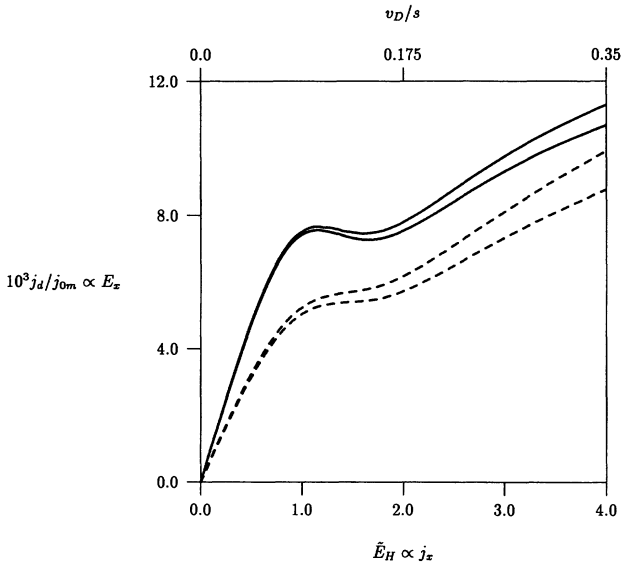

FIG. 1. Current-voltage characteristic for the PA (solid curves: $m = -1$) and DA (dashed curves: $m = 1$) interaction corresponding to Eq. (3) for $T = 1.7$ K, $B = 10$ T, $s = 7.1 \times 10^5$ cm/sec, and $m^* = 0.07m_0$; further, $g = 68$, $\tilde{\Delta} = 26$, $x_T = 3.84$, $D = \Omega^2/\tilde{\omega}^2 = 0.005$, and $\eta \approx 1.1$. The upper solid and dashed curves correspond to $t = 2$, the lower ones to $t = 1$. Here $j_{0m} = |e|\omega_c c'/(4\pi^2\hbar sm^*\tilde{\omega}^2 W\tilde{\ell}^{m+4})$ and $\tilde{E}_H = 1$ corresponds to $E_H = 62$ V/cm.

In Fig. 2 we represent CVC's for the same conditions as in Fig. 1 except for the temperature T which is twice smaller ($T = 0.85$ K). We have $g = 136$, $\tilde{\Delta} = 52$, and $x_T = 7.68$. From Eq. (8) we obtain that $\bar{E}$ lies close to the beginning of the NDC region in Fig. 1 and to its center in Fig. 2. Notice that in Fig. 2 for PA phonons we have NDC for minimum v_D at least 20% smaller than in Fig. 1. A comparable reduction is seen for the maximum v_D pertaining to the NDC region. The total width of the latter is almost unchanged as it should be for the case corresponding to Eq. (10). Moreover, we see that NDC has appeared in the corresponding low-voltage region for interaction with DA phonons. We empasize that for the most interesting regions in Figs. 1 and 2, the CVC can be calculated only numerically. Nevertheless, an analytical treatment shows that decreasing T favors the appearance of NDC due to a more abrupt suppression of the dissipation at the left edge of the channel. Figures 1 and 2 clearly lend support to such a conclusion. For not too large $x_T \lesssim 3$, Eq. (9) gives only order of magnitude estimate of ΔE. Thus, for $x_T \sim 1$ the dependence of ΔE on T should become much weaker than linear. This can be seen by comparing the curves for PA phonons in Figs. 1 and 2. According to the estimate given by Eq. (9) the width of the NDC region in Fig. 2 should be twice smaller than that of Fig. 1. This is obviously not the case. A more elaborate treatment gives for $x_T^2 \gg 10^2$ an additional logarithmic factor $\ln x_T^3$ to the estimate given by Eq. (9). Finally, for $x_T > 3$ we estimate $\Delta\tilde{E} = \Delta E/(\hbar\Omega^2/|e|\omega_c\tilde{\ell})$ as

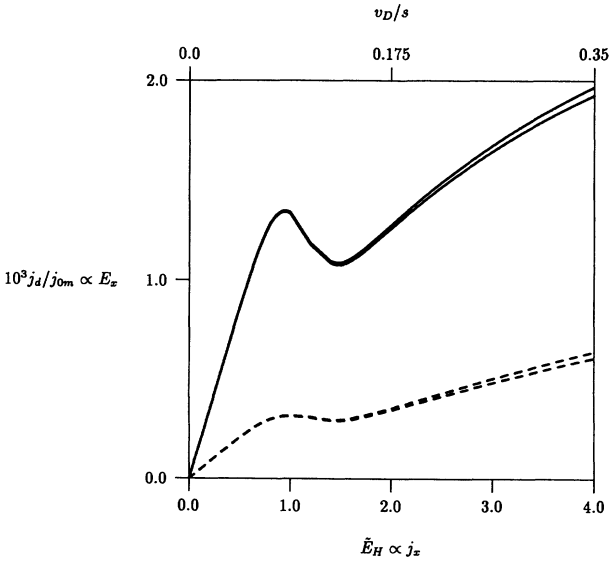

FIG. 2. Same as in Fig. 1 for $T = 0.85$ K ($g = 136$, $\tilde{\Delta} = 52$, $x_T = 7.68$).

$$\Delta\tilde{E} = \frac{1}{x_T}\left(1 + \frac{3x_T^2}{x_T^2 + 10^2}\ln x_T\right). \tag{11}$$

For $x_T^2 \gtrsim 10^2$ the logarithmic factor is related with a power-series decrease, approximately $\propto T^3$ (both for PA and DA phonons), of the contribution to the total dissipation from the left edge of the channel, when T decreases, for the Hall fields inside the region determined by Eqs. (8) and (11). This decrease is in addition to the usual temperature behavior. When $E_e/E_s \geq 1$, for low temperatures $x_T \gg 1$ the dissipation varies[7] as $\sim T^3$ for PA phonons and as $\sim T^5$ for DA phonons. For $x_T \gg 1$, similar dependences on T were obtained for the dissipation of a degenerate 3D-electron gas which occupies only the $N = 0$ Landau level and interacts with PA or DA phonons.[16] Further, from a comparison of Figs. 1 and 2, for E_H outside the region determined by Eqs. (8) and (11), we see that $j_d \sim T^3$ for PA phonons and $j_d \sim T^5$ for DA phonons. Also, the curves for $t = 3$ will practically coincide with those for $t = 2$.

The conditions used in Figs. 1 and 2 compare rather well with the experimental ones in Refs. 1 and 9 (see also Secs. IV and V). It is seen from Figs. 1 and 2 that we have the breakdown of the almost "dissipationless" current for $\min v_D \lesssim 0.09s \approx 6.4 \times 10^4$ cm/sec. This value of v_D is in good agreement with the experimental one.[1,9] This result lifts a ban, on a substantial role of acoustic emission in the breakdown in Si-MOS structures, stated in Ref. 9 since it contradicted earlier models that predicted $v_D \geq s$. The ban was based on an experimentally determined average drift velocity v_D that was much smaller [about 5×10^4 cm/sec (Refs. 1 and 9)] than the speed of sound in silicon.[9] We note in passing that some of the results of Ref. 9, show clearly a section with negative differential resistance.

In Fig. 3 the same curves as in Fig. 1 are represented for substantially wider regions of current densities j_x ($\propto \tilde{E}_H$). Because of an abrupt increase of the dissipation at $E_H/E_s \approx E_e/E_s + 1 \cong 2.1$, we represent CVC's in Fig. 3 for comparatively low fields and in Fig. 4 for larger $\tilde{E}_H$. As seen from Figs. 1 and 3, one CVC can have three different regions of NDC: (i) for $E_H/E_s \approx E_e/E_s - 1 \cong 0.1$, (ii) for $E_e/E_s + 1 > E_H/E_s > 1$, and (iii) for $E_H/E_s > E_e/E_s + 1 \cong 2.1$. Notice that in case (iii) the dissipation is practically independent of T (for $x_T > 1$) because a finite phonon emission at the right edge of the channel takes place even for $T = 0$, when phonon absorption is absent. In the transition region from (ii) to (iii), the CVC can be calculated only numerically. As can be seen, in this region the dissipation increases sharply by about two orders of magnitude. For the PA interaction in (iii) with $\eta = E_e/E_s > 1$, $x_T^2/2 > 1$, and $\eta_\pm = (E_H \pm E_e)/E_s$, we have $E_H - E_e > E_s$. Then assuming $[\eta_-^2 - 1]^2 \ll 1$, we obtain

$$j_d = \Gamma\sqrt{\pi}[2 + \lambda_+(\eta_-^2 - 1)]^{-3/2}\ , \tag{12}$$

where $\Gamma = |e|\omega_c c'/2\pi^2\hbar^2 s\tilde{\ell}\tilde{\omega}W$. The corresponding curves in Fig. 4 agree rather well with Eq. (12). For large t (smaller thickness of the 2DEG) we have a slower decrease as predicted by Eq. (12).

In contrast with Figs. 1–4, where $\eta > 1$, the results represented in Fig. 5 correspond to $\eta < 1$. All curves in Fig. 5 are for interaction with PA phonons in a GaAs/(AlGa)As heterostructure with $m^* \approx 7 \times 10^{-29}$ g, $s \approx 2.5 \times 10^5$ cm/sec. For curves 1–4 we suppose $B \approx 11$ T. Curves 1 and 2 are for $T = 0.95$ K, and curves 3 and 4 for $T = 1.9$ K. Curves 1 and 3 correspond to $\eta = 0.8$, with $D = 10^{-4}$, and curves 2 and 4, with $D = 5.625 \times 10^{-5}$, to $\eta = 0.6$. Notice that the vertical axis ($\propto E_x$) is logarithmic. We can see from Fig. 5 that for $E_H/E_s < 1 - \eta$ with increasing E_H we have a linear increase of $\log_{10}E_x$, the angle of which becomes larger for smaller T. Thus, for curves 1–4 we have, for $E_H/E_s < 1 - \eta$, the following dependence on E_H, T, and η

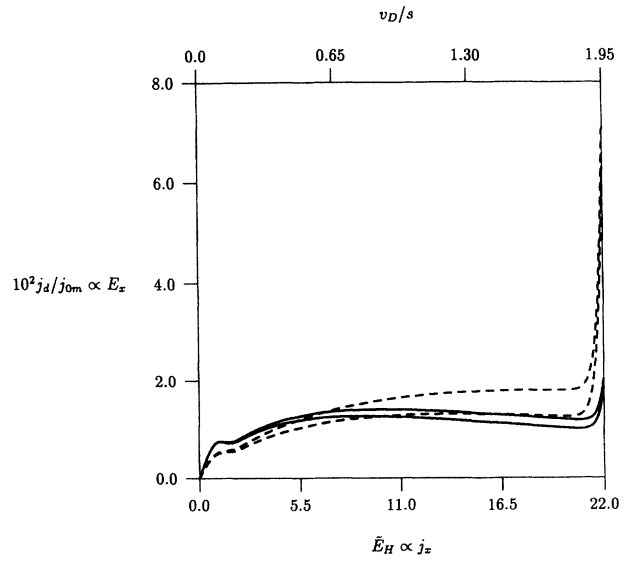

FIG. 3. Same as in Fig. 1 for a larger region of the current density j_x.

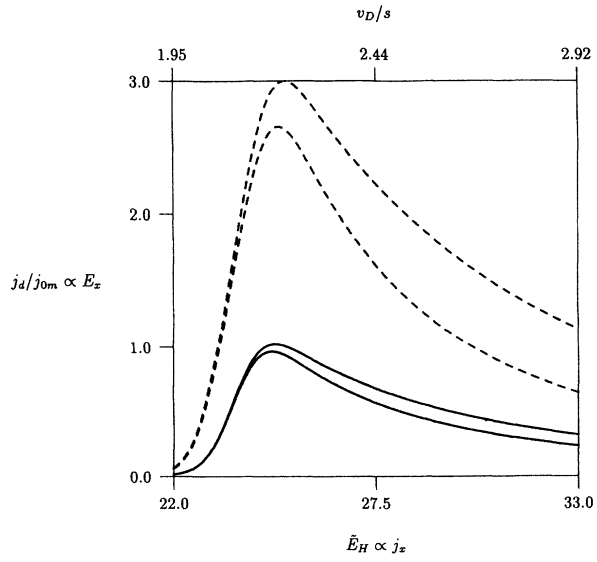

FIG. 4. Same is in Fig. 3 for another region of the current density. Notice the difference (10^2) in the vertical scales of these figures.

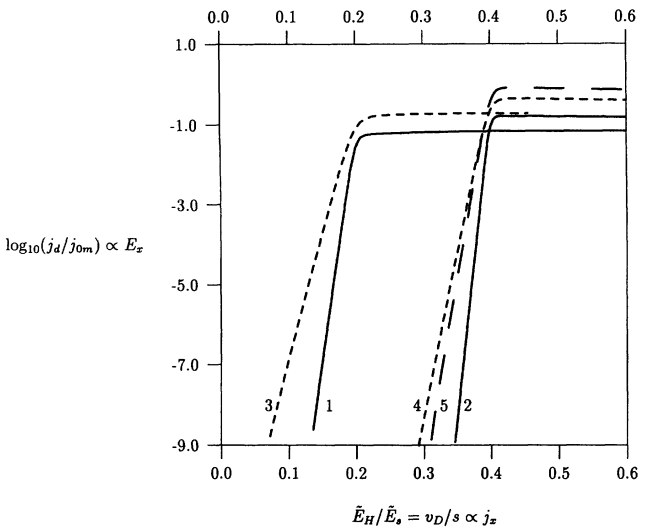

FIG. 5. Current-voltage characteristic for the PA interaction in a GaAs/(AlGa)As heterostructure ($m^* = 0.07m_0$, $s \approx 2.5 \times 10^5$ cm/sec), with $m = -1$, corresponding to Eq. (3) for $t = 1$. Curves 1–4 are for $B = 11$ T; curves 1 and 2 are for $T = 0.95$ K and 3 and 4 for $T = 1.9$ K. Curves 1 and 2 ($g = 200$, $\tilde{\Delta} = 100$, $x_T = 2.5$) correspond to $\eta = v_g/s = 0.8$ ($D = 10^{-4}$) and $\eta = 0.6$ ($D = 5.625 \times 10^{-5}$), respectively. Curves 3 and 4 ($g = 100$, $\tilde{\Delta} = 50$, $x_T = 1.25$) correspond to $\eta = 0.8$ ($D = 10^{-4}$) and $\eta = 0.6$ ($D = 5.625 \times 10^{-5}$), respectively. Curve 5 ($g = 40$, $\tilde{\Delta} = 60$, $x_T = 0.75$; $B = 3.78$ T, $T = 1.9$ K, $E_s \approx 95$ V/cm) corresponds to $D = 4.2 \times 10^{-5}$ and $\eta \approx 0.60$. The parameters pertain to the experiments of Ref. 2 and $\tilde{E}_H/\tilde{E}_s = v_D/s$.

$$j_d/j_{0,-1} \propto E_x \propto \exp(a|e|E_H/\eta k_B T), \tag{13}$$

where $a = (6.5 \pm 0.25) \times 10^{-5}$ cm and $j_{0m} = |e|\omega_c c'/(4\pi^2 \hbar s m^* \tilde{\omega}^2 W \tilde{\ell}^{m+4})$. Qualitatively, Eq. (13) compares well with the empirical relation observed in Ref. 2 for some other conditions ($\nu = 4$, $B = 3.78$ T) for different E_H and temperatures. For $E_H/E_s > 1 - \eta$, the curves 1 and 2 compare well with the analytical treatment of Ref. 7. Because of the very flat behavior of the CVC for $0.23 < E_H/E_s < 0.60$, for curve 1 the beginning of the NDC region is substantially better obtained (at $E_H/E_s \approx 0.48$) than in the corresponding curve in Fig. 4 of Ref. 7.

To treat the observed[2] increase of dissipation by approximately two orders of magnitude (from $\sigma_{xx} \sim 10^{-9}$ ohm^{-1} to $\sigma_{xx} \sim 10^{-7}$ ohm^{-1}; $\sigma_{xx} \approx \rho_{xx}\sigma_{xy}^2 = j_d/E_H$) at $T = 1.9$ K, $B = 3.78$ T ($\nu = 4$) for E_H in the interval from $\cong 38$ V/cm to $\cong 40$ V/cm, for which $\ln E_x \propto E_H$ [as in Eq. (13)], we suppose that it is related with intralevel transitions at the "edges" of the $N = 0$ Landau level. Transitions take place due to interaction with PA phonons. That is, we will assume that the intralevel contribution from the $N = 1$ Landau level and the interlevel contributions are not essential. Indeed, to be in accordance with other experimental results on this sample, we should assume $E_{e0}/E_s \cong 0.60$ (in E_{eN} the subscript N denotes the $N = 0$ or 1 Landau levels). Then $E_{e1}/E_s \approx 0.6/\sqrt{3} \cong 0.35$ if we assume the same effective confining potential for the $N = 1$ and $N = 0$ Landau levels, where $E_s \cong 94.5$ V/cm. Hence, for $E_H/E_s < 1 - E_{e1}/E_s \approx 0.65$ the intralevel contribution from the $N = 1$ Landau level should be exponentially small and at least negligible for $E_H/E_s \leq 1 - E_{e0}/E_s \approx 0.40$. For simplicity we neglect spin splitting. As regards the interlevel contribution, it can be neglected for $\Omega^2/\tilde{\omega}^2 \ll 1$ and relatively small E_H and temperature . Then, using Eq. (3), we obtain curve 5 in Fig. 5 with $g = 40$, $\tilde{\Delta} = 60$; $D = 4.2 \times 10^{-5}$ and $x_T = 0.75$. This curve shows the exponential behavior of Eq. (13), with $a/\eta \approx 3.8 \times 10^{-4}$ cm; this value compares well with the observed one.[2] It is interesting to compare the order of magnitude of the dissipation in this region, curve 5 in Fig. 5, with the experimental curve.[2] For usual parameters $c' = \hbar(eh_{14})^2/2\rho s$, $h_{14} = 1.2 \times 10^7$ V/cm, and $\rho = 5.31$ g/cm^3, we obtain $\sigma_{xx} \approx 7.4 \times 10^{-9}(E_s/E_H) j_d/j_{0,-1}$ ohm^{-1}, where we have used the potential V_y', since $W = 50$ μm, and included a spin factor 2 . Here the preexponential factor is only about 5 times smaller than necessary for agreement with the experimental result. We consider this difference, for such approximate treatment, as nonessential. Notice that for $E_H/E_s > 0.44$ (i.e., $E_H > 41.6$ V/cm) curve 5 represents NDC, i.e., breakdown of the weakly dissipative regime of the quantum Hall effect.[7]

With regard to curve 5 in Fig. 5, the important assumption $\eta < 1$ for all occupied Landau levels in the experiment of Ref. 2 (for $B = 3.78$ T) is well justified from Fig. 2 of this work: for $B = 3.78$ T and a small $E_H = 2.5$ V/cm, the experimental curve shows clearly an exponential dependence of dissipation on $1/T$ with a rather large activation energy (2.26 meV) for $T < 4$ K. Indeed, for $\eta \geq 1$ the intraedge-channel contribution to dissipation should be $\propto T$ (notice that $x_T < 1$ in Fig. 2, Ref. 2) for E_H between zero and at least $E_H \lesssim 100$ V/cm for the present parameters.

IV. ANISOTROPIC ELECTRON-PHONON INTERACTION

In this section we consider the CVC for interaction with LA and TA phonons in Si(100) MOS structures. As we will show, the 2DEG interacts substantially with both kinds of phonons. We will treat in more detail the observations of Refs. 1 and 9. Below, supposing $\eta > 1$, we will treat only the low-voltage CVC's ($v_D < s$) related with the suppresion of dissipation at the left edge of the channel and the dependendence of the electron-phonon interaction on the typical angle θ, counted from the z axis, of the wave vector of phonons which provide the most substantial contribution to dissipation.

In Fig. 6 we plot the CVC's for interaction with LA phonons (solid curves 1–3) for $T \simeq 1.5$ K, $B \simeq 10$ T, $m^* = 0.19m_0$, $D = 0.02$, and $s \simeq 8.4 \times 10^5$ cm/sec, in the low-voltage region. We have $\tilde{\Delta} = 10$, 20, and 30 for curves 1 and 4, 2 and 5, and 3 and 6, respectively. In addition, $g = 40$, $x_T = 5.13$, $\tilde{E}_s = 6.41$. For the same parameters, we show the curves 4–6 (dashed) for isotropic electron-phonon interaction. For DA phonons we represent j_d/j_{01} and for LA phonons the dimensionless value j_d/j_{0L}, where $j_{0L} = |e|\omega_c B_{0L}/(4\pi^2 \hbar s_L m^* \tilde{\omega}^2 W \tilde{\ell}^5)$.

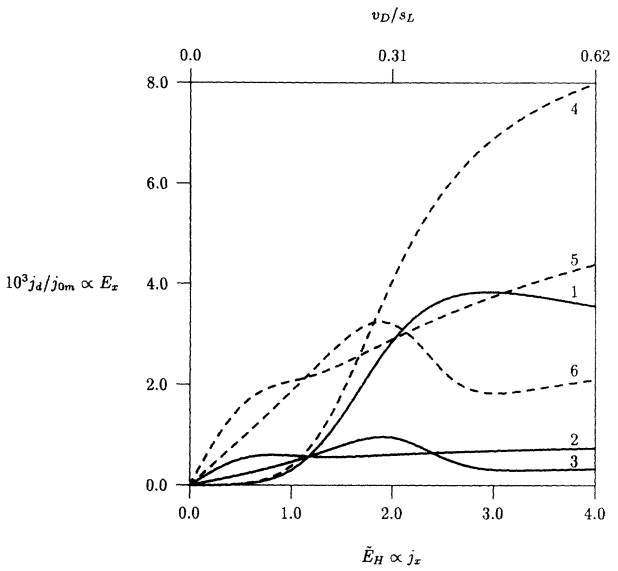

FIG. 6. Current-voltage characteristic corresponding to Eq. (7) (solid curves 1–3) and to Eq. (3) (dashed curves 4–6) for $T \simeq 1.5$ K, $B \simeq 10$ T, $m^* = 0.19m_0, D = 0.02$, $s_L = s = 8.4 \times 10^5$ cm/sec, $t = 1$, $g = 40$, $D = 0.02$, $x_T = 5.13$, and $E_s = 6.41$. The solid (dashed) curves correspond to interaction with LA phonons (DA phonons). For curve 4 the units are $5 \times 10^2 j_d/j_{01}$ and for curves 1–3 $10^3 j_d/j_{0L}$, where $j_{0L} = |e|\omega_c B_{0L}/(4\pi^2 \hbar s_L m^* \tilde{\omega}^2 W \tilde{\ell}^5)$.

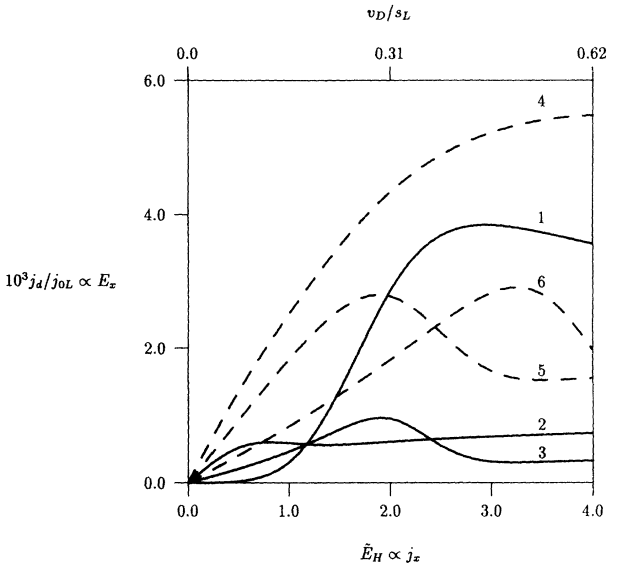

FIG. 7. Current-voltage characteristic corresponding to Eq. (7). The solid curves (1–3) correspond to interaction with LA phonons ($s_L = 8.4 \times 10^5$ cm/sec, $x_{TL} = 5.13, \tilde{E}_{sL} = 6.41$) and the dashed curves (4–6) to interaction with TA phonons ($s_T = 5.8 \times 10^5$ cm/sec, $x_{TT} = 3.54$). The other parameters are the same as in Fig. 6. Curves 1 and 4 correspond to $\tilde{\Delta} = 10$, curves 2 and 5 to $\tilde{\Delta} = 20$, and curves 3 and 6 to $\tilde{\Delta} = 30$.

Curve 4 shows no NDC whereas curve 1 does in addition to showing a much slower increase above $\tilde{E}_H \approx 1.0$. That is, the anisotropy causes the appearence of NDC. It is due to the factor $(-2/3 + \cos^2\theta)^2$, which decreases with increasing E_H for $\tilde{E}_H \geq 2$ under the stated conditions. Notice that curves 1 and 4 are for $\eta \approx 0.78$ and for $\tilde{E}_H \leq (1-\eta)\tilde{E}_s \approx 1.4$ we have a strongly nonohmic behavior (compare with Fig. 5). Curve 2 shows NDC for very small fields E_H ($0.8 \leq \tilde{E}_H \leq 1.4$) that as a result of the anisotropy. Indeed, for curve 5 NDC is absent but in the same region the CVC becomes rather flat. The typical Hall field for this region is well estimated by Eq. (8). Thus the breakdown of the weakly dissipative quantum Hall regime due to NDC here is possible for much smaller ratios $E_H/E_s \approx 0.12$ than for $\tilde{\Delta} = 10$. For $\tilde{\Delta} = 30$, curves 3 and 6 have the same qualitative behavior; here NDC appears for E_H/E_s more than twice larger than for $\tilde{\Delta} = 20$ in accordance with Eq. (8). The peak-to-valley ratio in the NDC region of curve 3 is approximately 1.8 times larger than the corresponding value of curve 6. Since all parameters are the same for both curves this increase results from the anisotropy of the interaction.

The numerical results represented in Fig. 7 correspond to the same conditions as those in Fig. 6; the only difference is that the dashed curves correspond to interaction with TA phonons, obtained from Eq. (7). Here we have $x_{TL} = 5.13$, $x_{TT} = 3.54$. Notice that for $\tilde{\Delta} = 10$, due to the difference in speed s between the LA and TA phonons, for LA phonons $\eta < 1$ and dissipation due to them is negligible at the left edge of the channel, while the opposite holds for TA phonons. In addition, curve 4 shows no NDC whereas the corresponding curve 1 does. For curves 2 and 5 ($\tilde{\Delta} = 20$), the corresponding maximum values of $\tilde{E}_H$ are substantially different: ≈ 0.80 for LA and ≈ 1.80 TA phonons. Such a substantial difference for the onset of NDC also takes place when $\tilde{\Delta} = 30$, see curves 3 and 6 in Fig. 7. From Fig. 7 it is seen that interaction with TA phonons can play the main role in the occurence of NDC and is in competition with the contribution of the LA phonons. Note that for TA phonons we can obtain substantially lower Hall fields for breakdown with other $\tilde{\Delta}$. For instance, if $\tilde{\Delta} = 15$ we obtain NDC in the region $1.3 \leq \tilde{E}_H \leq 2.3$.

The numerical results represented in Fig. 8 correspond to the same conditions and notations as those in Fig. 7 except for the temperature, $T = 0.5$ K. We have $g = 120$, $x_{TL} = 15.39$, $x_{TT} = 10.62$; the corresponding values for $\tilde{\Delta}$ are three times larger. In comparison with curve 2 of Fig. 7, curve 2 in Fig. 8, that corresponds to interaction with LA phonons for $\tilde{\Delta} = 60$, shows a substantially larger peak-to-valley ratio in the NDC region; the latter starts at lower voltage and is narrower. However, in contrast with curve 1 in Fig. 7 showing NDC due only to the anisotropy, for $\tilde{E}_H > 3$, curve 1 in Fig. 8 shows no NDC; we have almost a constant dissipation due to LA phonons with increasing j_x. Curves 3 and 5, in Figs. 7 and 8, show the same qualitative behavior. The typical values of dissipation in Fig. 8 are approximately 120 times smaller than in Fig. 7. This is in line with the discussion above and the dependence $\propto T^5$.

In Fig. 9 we represent CVC's that correspond to the sum of the LA and TA phonon contributions to dissipation for the cases represented in Figs. 7 and 8. For

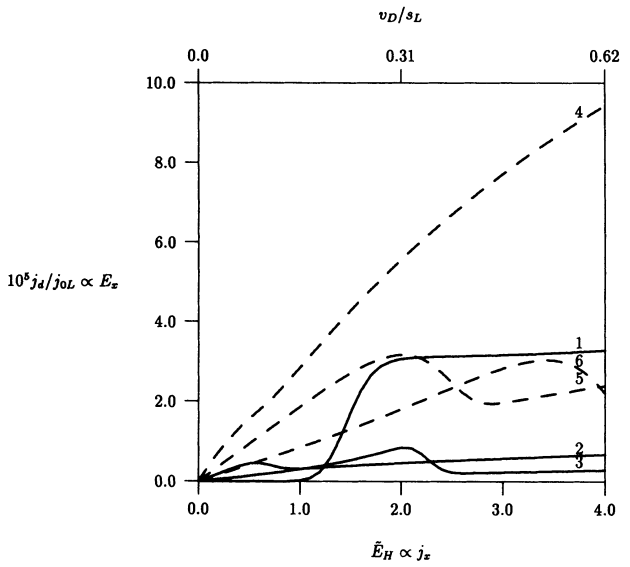

FIG. 8. Current-voltage characteristic corresponding to Eq. (7) for $T = 0.5$ K. The solid curves (1–3) correspond to interaction with LA phonons ($x_{TL} = 15.39$) and the dashed curves (4–6) to interaction with TA phonons ($x_{TT} = 10.62$). The other parameters are the same as in Fig. 6. The $\tilde{\Delta}$ assignment of the curves is the same as in Fig. 7 and the $\tilde{\Delta}$ values three times larger.

$g = 40$, the region of NDC for $\tilde{\Delta} \approx 15$ has the minimum $\tilde{E}_H$ about twice smaller than in Fig. 8, see also the discussion of Fig. 7. Notice that in curve 6 a new region of NDC, at $\tilde{E}_H \approx 2.1$ has appeared in comparison with the corresponding high-temperature curve 3.

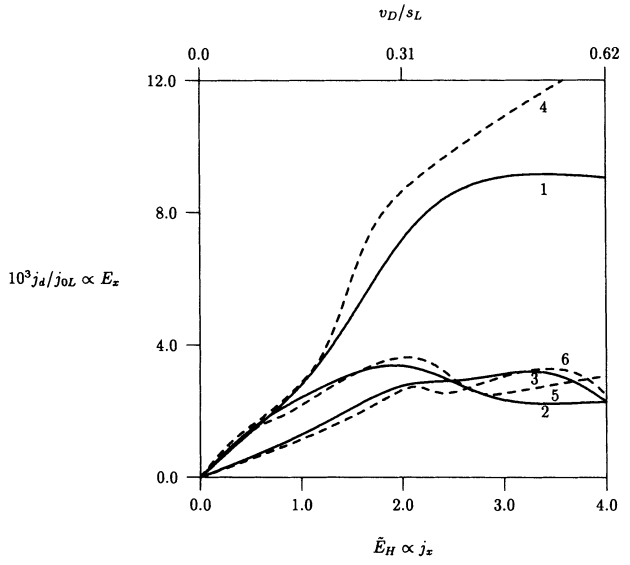

FIG. 9. Sum of the LA and TA phonons contributions to the current-voltage characteristic for the cases represented in Fig. 7 (solid curves 1–3) and in Fig. 8 (dashed curves 4–6). The dashed curves have been multiplied by an additional factor 10^2. Curves 1–6 are obtained with $\tilde{\Delta} = 10, 20, 30, 30, 60$, and 90, respectively.

V. DISCUSSION AND CONCLUDING REMARKS

One of the main results of this paper is the qualitatively different behaviors of the CVC's of narrow channels at the beginning of the low-voltage region, that includes E_H (or j_x) just above zero, for (i) $E_e \geq E_s$ and (ii) $E_e < E_s$, cf. Ref. 17. This is seen, e.g., by comparing the ohmic behavior of the CVC's in Fig. 1 for $v_D/s \ll 0.1$ with that for small v_D/s in Fig. 5. The results depend strongly on the parameter Ω characterizing the smoothness of the confining potential. This is practically the only unknown parameter in our model that is necessary to compare the theoretical with the experimental results. However, our study shows that such an uncertainty in Ω can be reduced substantially since the range of Ω values can be deduced from the usual measurements such as those of Ref. 2. In particular, our results, as well as those of Ref. 7, show the possibility of an exponentially strong suppression $\sim \exp[-\tilde{\Delta}(1-\eta^2)/\eta^2]$ of intralevel inelastic scattering due to acoustical phonons. For the experimental conditions of Ref. 2 discussed above, this suppression is stronger than $\exp(-\hbar\omega_c/k_BT)$. This in sharp contrast with the results of Refs. 18 and 19 that do not show any possibility of such a strong exponential suppresion. Notice that $\eta = E_e/E_s \equiv v_g/s$, where v_g is the group velocity of an edge state. In all figures, because of $\Omega \ll \omega_c$ we have $\tilde{\omega} \approx \omega_c$ and $\tilde{\ell}$, in $t = \tilde{\ell}^2/\ell_z^2$, almost coincides with the magnetic length. Moreover, ℓ_z is approximately equal to the thickness of the 2DEG. Assuming a sufficiently smooth confinement, such that $v_g/s \approx 0.6$, we have obtained good agreement with the observed[2] strong exponential increase in the dissipation for small increase in E_H (before the breakdown). This is clear by comparing curve 5 in Fig. 5 with the corresponding results of Ref. 2 and has been detailed in Sec. III.

The activated temperature dependence of the resistivity minimum in Fig. 1 of Ref. 1 (from $T \approx 4.2$ K to $T \approx 2.7$ K), for $B = 10.3$ T does not contradict our assumption $E_e > E_s$. This is because (i) for $T = 3.3$ K and $B \approx 10$ T the contribution from the edges to the total resistivity should be at least two orders of magnitude smaller than the observed value of the resistivity, related most likely with the contribution of the inner part of the channel, and (ii) the breakdown was perfectly observed for $T = 1.5$ K, when the inner contribution should be $\approx 3 \times 10^{-6}$ times smaller than that for $T = 3.3$ K but the edge-intralevel contribution only ≈ 50 times smaller. Thus for $T = 1.5$ K the main contribution to the total dissipation in the channel should result from intralevel transitions at the edges.

We have assumed a uniform Hall field in the channel. For not too low current densities j_x this complements rather well with the experiment of Ref. 20 in a GaAs/(AlGa)As heterostructure: for current densities $j_x \geq 10^{-2}$ A/m, a linear increase of the Hall voltage over the entire width of the sample was observed even in the center of the plateau ($\nu = 4$; $B \approx 5.1$ T, $T = 1.5$ K). The current density that corresponds to the region $E_H/E_s \approx 0.4$ in curve 5 in Fig. 5, is $j_x \approx 0.64$ A/m ($v_D \approx 1.1 \times 10^5$ cm/sec), i.e., j_x is practically two orders

of magnitude larger than j_x for which in Ref. 20 an almost linear increase of the Hall potential over the sample width was measured. For a recent discussion of the spreading out of the current density in a Hall bar see Ref. 21. In this work even for a very small current and hard-wall confining potential, a substantial bulk current was obtained. For smooth confining potentials this speading out of the current density should be further enlarged.[21] This type of confining potential appears more realistic.[22,23]

Finally, we mention that a recent comprehensive numerical study[24] of anisotropic deformation potentials (for intravalley scattering) in Si emphasizes the difference between numerical results for $\Xi_{\rm TA}(\theta)$ and $\Xi_{\rm LA}(\theta)$ and those from analytical model.[11,14] The most important difference is related with at least 1.6 times smaller θ at wich $\Xi_{\rm TA}(\theta)$ has a maximum. This should lead to more pronounced NDC regions in the CVC's for $v_D/s \lesssim 0.1$ for the total contribution of both TA and LA phonons.

ACKNOWLEDGMENT

The work of one of us (P.V.) was supported by NSERC Grant No. OGPIN028.

[1] K. von Klitzing, G. Ebert, N. Kleinmichel, H. Obloh, G. Dorda, and G. Weimann, *The 17th International Conference on the Physics of Semiconductors, 1984* (Springer-Verlag, New York, 1985), p. 271.

[2] S. Komiyama, T. Takamasu, S. Hiyamizu, and S. Sasa, Solid State Commun. **54**, 479 (1985).

[3] P. C. van Son, G. H. Kruithof, and T. M. Klapwijk, Phys. Rev. B **42**, 11 267 (1990).

[4] E. I. Rashba and V. B. Timofeev, Fiz. Tekh. Poluprov. **20**, 977 (1986)[Sov. Phys. Semicond. **20**, 617 (1986)].

[5] *The Quantum Hall Effect*, edited by R. E. Prange and S. M. Girvin (Springer -Verlag, New York, 1987).

[6] O. G. Balev, Fiz. Tver. Tela, **32**, 871 (1990) [Sov. Phys. Solid State **32**, 514 (1990)].

[7] O. G. Balev and P. Vasilopoulos, Phys. Rev. B **47**, 16 410 (1993).

[8] V. G. Makerov, B. K. Medvedev, V. M. Pudalov, D. A. Rinberg, S. G. Semenchinskii, and Yu. V. Slepnev, Pisma Zh. Eksp. Teor. Fiz. **47**, 59 (1988) [JETP Lett. **47**, 71 (1988)].

[9] Yu. V. Dubrovskij, M. S. Nunuparov, and M. I. Reznikov, Zh. Eksp. Teor. Fiz. **94**, 356 (1988) [Sov. Phys. JETP **67** 632 (1988)] .

[10] *American Institute of Physics Handbook*, 3rd ed., edited by D. E. Gray *et al.* (McGraw-Hill, New York, 1972).

[11] G. A. Toombs, F. W. Sheard, D. Nelson, and L. J. Challis, Solid State Commun. **64**, 577 (1987).

[12] K.-F. Berggren, T. J. Thornton, D. J. Newson, and M. Pepper, Phys. Rev. Lett. **57**, 1769 (1986).

[13] P. Vasilopoulos, Superlatt. Microstruct. **5**, 583 (1989); K. F. Berggren, G. Roos, and H. van Houten, Phys. Rev. B **37**, 101 48 (1988).

[14] V. F. Gantmakhern and Y. B. Levinson, *Carrier Scattering in Metals and Semiconductors* (North-Holland, Amsterdam, 1987).

[15] G. Gradshteyn and I. M. Ryzhik, *Tables of Integrals, Series, and Products* (Academic, New York, 1965).

[16] P. S. Zyrianov and M. Klinger, *Quantum Theory of Electron Transport Phenomena in Crystalline Semiconductors* (Nauka, Moscow, 1976).

[17] This qualitative difference at small E_H has been taken into account in our previous study (Ref. 7).

[18] T. Martin and S. Feng, Phys. Rev. Lett. **64**, 1971 (1990).

[19] J. J. Palacios and C. Tejedor, Phys. Rev. B **44**, 8157 (1991).

[20] P. F. Fontein, P. Hendriks, F. A. P. Blom, J. H. Wolter, L. J. Giling, and C. W. J. Beenakker, Surf. Sci. **263**, 91 (1991).

[21] D. J. Thouless, Phys. Rev. Lett. **71**, 1879 (1993).

[22] S. Komiyama, H. Hirai, M. Ohsawa, and Y. Matsuda, Phys. Rev. B **45**, 11 085 (1992).

[23] R. J. F. van Haren, F. A. P. Blom, W. de Lange, and J. H. Wolter, Phys. Rev. B **47**, 15 700 (1993).

[24] H. Mizuno, K. Taniguchi, and C. Hamaguchi, Phys. Rev. B **48**, 1512 (1993).